Retrievals of Antarctic aerosol characteristics using a Sun-sky radiometer during the 2001–2002 austral summer campaign

C. Di Carmine and M. Campanelli
Istituto di Scienze dell'Atmosfera e del Clima, Consiglio Nazionale delle Ricerche, Rome, Italy

T. Nakajima
Centre for Climate System Research, University of Tokyo, Tokyo, Japan

C. Tomasi and V. Vitale
Istituto di Scienze dell'Atmosfera e del Clima, Consiglio Nazionale delle Ricerche, Bologna, Italy

Received 26 July 2004; revised 31 January 2005; accepted 1 April 2005; published 12 July 2005.

[1] In order to characterize the Antarctic aerosol and to analyze the effect of katabatic winds on the properties of suspended particles, measurements of solar direct and diffuse irradiance were carried out at the Italian Terra Nova Bay station in Antarctica, during the 2001–2002 austral summer campaign. Measurements were performed by the ground-based PREDE sky radiometer and processed by using the Skyrad inversion code. Aerosol optical thickness at 500 nm was found to vary between 0.01 and 0.02. The volume size distribution curves showed bimodal features with the two modes located within 0.1–0.3 μm and 5–7 μm radius intervals, respectively. The real part of the refractive index characterizing the Antarctic aerosol was found to have a mean value of 1.40. During the katabatic event the analysis indicated that the advection of larger and drier fresh particles, together with the removal of marine suspended particles, caused the decrease in aerosol optical thickness.

Citation: Di Carmine, C., M. Campanelli, T. Nakajima, C. Tomasi, and V. Vitale (2005), Retrievals of Antarctic aerosol characteristics using a Sun-sky radiometer during the 2001–2002 austral summer campaign, *J. Geophys. Res.*, *110*, D13202, doi:10.1029/2004JD005280.

1. Introduction

[2] Antarctica is considered an attractive site for studying aerosol properties, free from the noise due to atmospheric pollution. In fact, it is expected to have the cleanest air mass in the global atmosphere, being located in the Southern Hemisphere, where land areas are more limited and human activities are less developed. Air circulation over Antarctica also seems to prevent the direct transport of air originating from anthropogenic sources of pollution at the lower latitudes.

[3] Many instruments and techniques have been developed over the last twenty years to provide aerosol characterization [*Tanaka et al.*, 1986; *Holben et al.*, 1998; *Michalsky et al.*, 2001]. In particular, methods based on the use of sky radiometers measuring spectral direct and diffuse solar irradiance allow the retrieval of simultaneous columnar optical and physical properties of aerosol, using very compact instruments, and fast and efficient inversion algorithms [*King et al.*, 1978; *Nakajima et al.*, 1983; *Dubovik and King*, 2000].

[4] In Antarctica these techniques are still under study and development, with the purpose of resolving some difficulties in their application: First, only during a few months each year can the solar irradiance be measured, constituting a limitation to the monitoring of polar aerosol using passive optical measurements; second, the application of the above-mentioned models requires an approximation of plane parallel atmosphere, which is verified for high solar elevation, but not always in Antarctica; third, low temperature is another obstacle to the stable operation of the instrument.

[5] The first application of the sky radiance inversion technique is reported by *Shiobara et al.* [1987]: A PREDE sky radiometer was installed at the Japanese Syowa station in 1984, and data were processed by the Skyrad code [*Nakajima et al.*, 1983]. Their results suggest that the sky radiometer is capable of obtaining more information than the usually less sophisticated Sun photometer, as operated widely in the earlier period. In fact, sky radiometers using the inversion code can retrieve aerosol optical thickness, size distribution, refractive index and single-scattering albedo, whereas the traditional instruments measuring direct solar irradiance at different wavelengths can retrieve only the spectral patterns of aerosol optical thickness.

[6] In the present work, we present a recent application of the above technique, with improved instrumentation and inversion scheme. A PREDE-POM 01L sky radiometer was installed at the Italian Terra Nova Bay (TNB) station from

0148-0227/05/2004JD005280$09.00

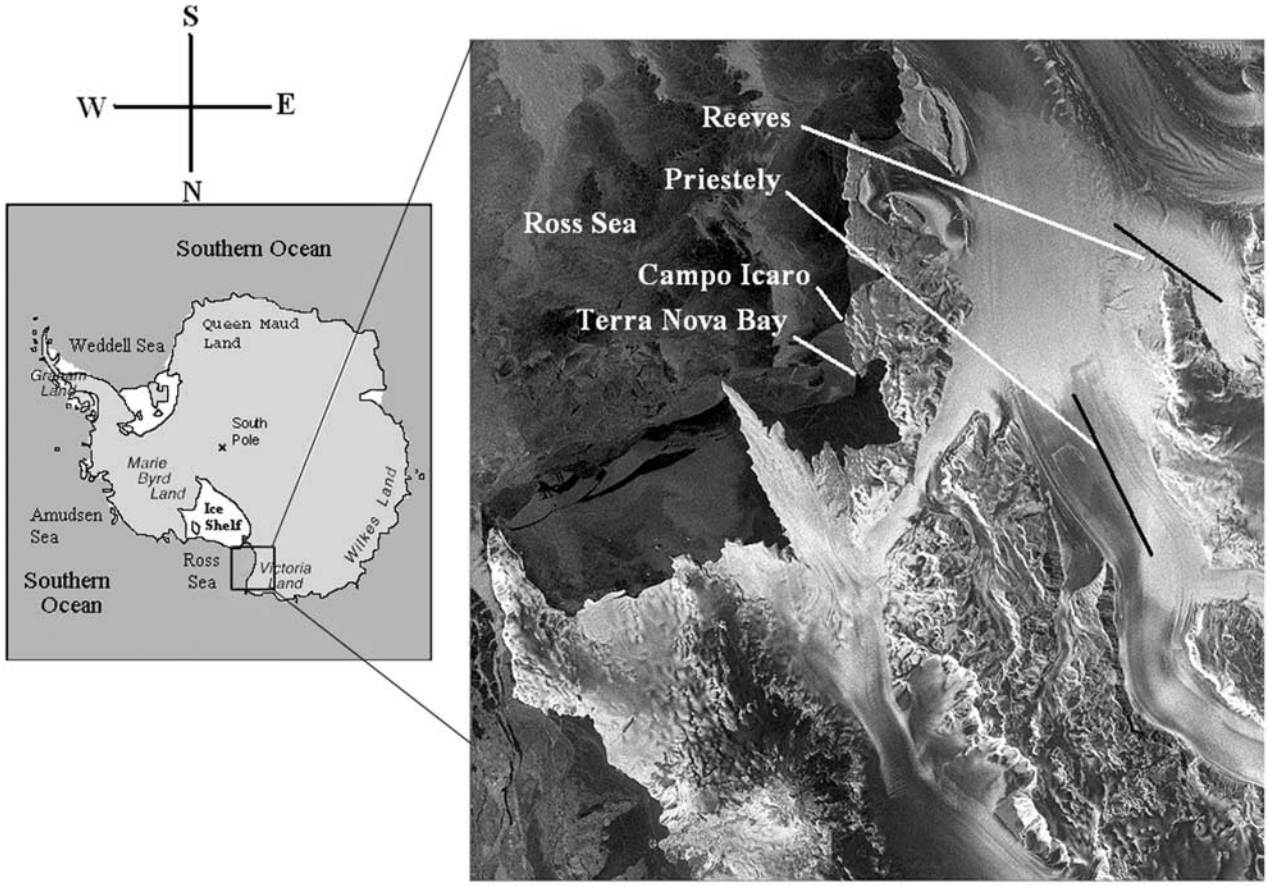

Figure 1. (left) Map of Antarctica with the overall location of the Terra Nova Bay coastal area on the Ross Sea. (right) A radar view of the measurement site.

1999 to 2001, and the data acquired in the Antarctic summer period of 2000–2001 were processed using the Skyrad code version 3 [*Nakajima et al.*, 1996; *Campanelli et al.*, 2004]. The aim of this paper is to characterize the Antarctic aerosol and to analyze the effect of katabatic winds on the properties of airborne particles.

2. Experimental Site and Measurements

[7] In order to characterize the Antarctic aerosol, measurements of solar irradiance were carried out at the Italian Antarctic base located at TNB on the northern coast of Victoria Land on the Ross Sea (Figure 1). Data were collected during the 2001/2002 Antarctic campaign from 30 November to 5 February. Measurements were performed by the ground-based PREDE sky radiometer, model POM-01L, which measured the sky-diffuse irradiance and direct solar irradiance at four wavelengths in the visible and near-infrared range (400 nm, 500 nm, 870 nm and 1020 nm), in the Almucantar geometry [*Tonna et al.*, 1995]. The wavelengths were carefully selected within the main windows defined by the numerous gaseous absorption bands characterizing the solar spectrum, using a series of narrowband interference filters manufactured by Hamamatsu with half-bandwidth of 10 nm, this choice allowing us to reduce the radiative transfer problem in the atmosphere to a purely scattering problem. The interior temperature of the sky radiometer was maintained at a temperature of 23°C by electric heaters.

[8] Meteorological data were recorded by the AWS Eneide station of the PNRA Meteo-climatological Observatory, located at TNB. In particular, (1) temperature was measured by means of the temperature probe (VAISALA DTS12 model), with a precision of ±0.13°C at −50°C; (2) relative humidity was measured by means of a HUMICAP capacitor, manufactured by VAISALA, with a precision of ±2%; (3) wind direction was measured by a counterbalanced optoelectronic wind vane (VAISALA WAV 15A model), with a precision of about ±2.8 degrees and a low threshold of 0.3 m/s; (4) wind speed was measured by means a low-threshold 3-cup optoelectronic anemometer (VAISALA WAA 15A model), having an accuracy of about ±2%, with a low threshold of 0.4 m/s.

[9] The PREDE sky radiometer was installed at the experimental site called Campo Icaro (74°42′56″S; 164°06′52″E), about 2 km south of the TNB station, at a height of 50 m above sea level, on a promontory whose surface is almost completely de-iced during the warmer months, as can be seen in Figure 1. However, it is not far from the Ross Sea to the west and from extensive ice fields to the east, formed by the convergence of the Reeves Glacier and the Priestley Glaciers. The promontory is characterized by heterogeneous soil morphology, with rocky formations mostly consisting of syenogranites presenting

reddish-brownish color, together with other metamorphic rocks and terrains rich in organic substances [*Zibordi and Meloni*, 1991].

[10] Although relatively close to the TNB station, the field station of Campo Icaro is negligibly affected by local anthropogenic influences; this is due to the orography and the local wind regime. In fact, the analysis of the wind field recorded by the nearby AWS Eneide station indicates that winds blow from the north (that is, from TNB) only in 5% of cases, whereas the prevailing wind direction is from the Priestley and Reeves Glaciers in more than 20% of cases. For our analysis, we also used backward trajectories (http://www.arl.noaa.gov) of 96-hour duration reaching Campo Icaro, produced with the HYSPLIT model provided over sea by the NOAA Air Resources Laboratory.

[11] During the campaign, higher temperatures were recorded than in the previous years. The mean temperature increased from −4°C to 6°C in December, and decreased from 4°C to −3°C throughout January and February. The highest values were measured from 27 December to 17 January, with the maximum varying between 6°C and 10°C on 11 and 12 January.

[12] Relative humidity (RH) values were found to fluctuate between 30% and 80% in December and January, and between 30% and 60% in February.

3. Processing Method

[13] The sky radiometer POM-01L takes measurements of direct solar irradiance F and sky-diffuse irradiance E at wavelengths of 400, 500, 870 and 1020 nm, both of which can be evaluated in W m^{-2} μm^{-1}. Irradiance F is given as

$$F = F_o \exp(-m_o\ \delta) \tag{1}$$

where F_o is the solar irradiance at the top of the atmosphere, retrieved by the improved Langley plot method [*Campanelli et al.*, 2004], m_o is the relative optical air mass approximately expressed as the inverse of the cosine of the solar zenith angle θ_o of the Sun, and δ is the total optical depth, which is the sum of aerosol and molecular optical depths.

[14] Sky-diffuse irradiance E is measured at several scattering angles, from 3° to 120°, in the Almucantar geometry, i.e., along a conical surface with constant zenith angle θ_o and letting azimuth angle ϕ vary. Before processing, the data were selected in order to choose only measurements taken for clear sky conditions. This was done because the inversion scheme used to process data assumes that the contribution of scattering and absorption is due to aerosols only, and does not consider the presence of cloud radiative effects. For this purpose, a cloud screening procedure was adopted, based on the following criteria: (1) careful check of the measurements of total global radiation reaching the ground, performed simultaneously with a Kipp and Zonen pyranometer, model CM 11, in order to discover the scattering effects produced by clouds close to the Sun; (2) examination of the direct solar irradiance measurements taken with the PREDE, to discard the measurements presenting significant drops due to cloud extinction from the time patterns of the logarithms of monochromatic direct solar irradiance versus local time, and (3) selection of the field measurements in terms of the ratio between diffuse and direct irradiance values taken at different angular distances from the solar disk: The data were rejected in all cases where the shape of the angular curve of the above ratio was found to be irregular, with discrepancies greater than 5% for angular distances >5° and 10% for angular distances ≤5°.

[15] Both direct and diffuse measured irradiances were processed using the Skyrad code developed by *Nakajima et al.* [1996]. Using an iterative scheme, the code is able to retrieve the aerosol optical thickness $\tau(\lambda)$, the columnar aerosol volume distribution $v(r) = dV/dln\ r$ (defined as the aerosol volume V in the vertical atmospheric column of unit cross section per unit interval of the particle radius logarithm), the phase function $P(\lambda, \Theta)$ and the single-scattering albedo $\omega(\lambda)$ from the measured normalized irradiance, expressed in the following form:

$$R(\lambda, \Theta) = \frac{E(\lambda, \Theta)}{\Delta\Omega(\lambda) F(\lambda) m_o} \tag{2}$$

where $\Delta\Omega(\lambda)$ is the solid viewing angle of the instrument.

[16] The calibration constant $\Delta\Omega(\lambda)$ in equation (2) was retrieved by means of the solar disk scanning method [*Boi et al.*, 1999]. Only data corresponding to air mass values smaller that 4.5 where considered.

[17] The normalized radiance $R(\lambda, \Theta)$ was determined as the solution of the radiative transfer equation [*Nakajima and Tanaka*, 1986, 1988], its expression in the Almucantar geometry for a one-layer plane parallel atmosphere being given by

$$R(\lambda, \Theta) = \omega(\lambda)\tau(\lambda)P(\lambda, \Theta) + q(\lambda, \Theta) = \beta(\lambda, \Theta) + q(\lambda, \Theta) \tag{3}$$

where $q(\lambda, \Theta)$ is the multiple-scattering contribution and $\beta(\lambda, \Theta)$ is the total differential scattering contribution for the single scattering. From the spectral values of R, the scattering coefficient β can be obtained by means of an iterative scheme. The aerosol volume distribution can then be derived from β and τ data and used in turn to reconstruct τ and β and, consequently, R. The iteration procedure stops when parameter ε_R turns out to be lower than 1% or, in other cases where this condition is not satisfied, after a certain number of loops established a priori by the user. Parameter ε_R is the RMS relative deviation between the measured and the reconstructed data of normalized radiance R and can be considered a reliable measure of the accuracy provided by the retrieval process.

[18] In order to retrieve accurate results, the Skyrad code needs to use the refractive index $\tilde{m} = m - i\ k$ and ground albedo A as input parameters. In determining the refractive index, two inversion modalities can be followed: The first requires a fixed value of the refractive index, while the second retrieves it from the data themselves. In the latter case, parameters m and k are retrieved simultaneously through a two-dimensional nonlinear search method: It was used to invert data in the present analysis.

[19] The ground albedo A was assumed to be equal to 0.4 at Campo Icaro. The rocky terrain was evaluated by *Tomasi et al.* [1990] as presenting values of albedo increasing from about 0.1 at the 400 nm wavelength to more than 0.4 at wavelengths beyond 1 μm, with a mean value of 0.20 at

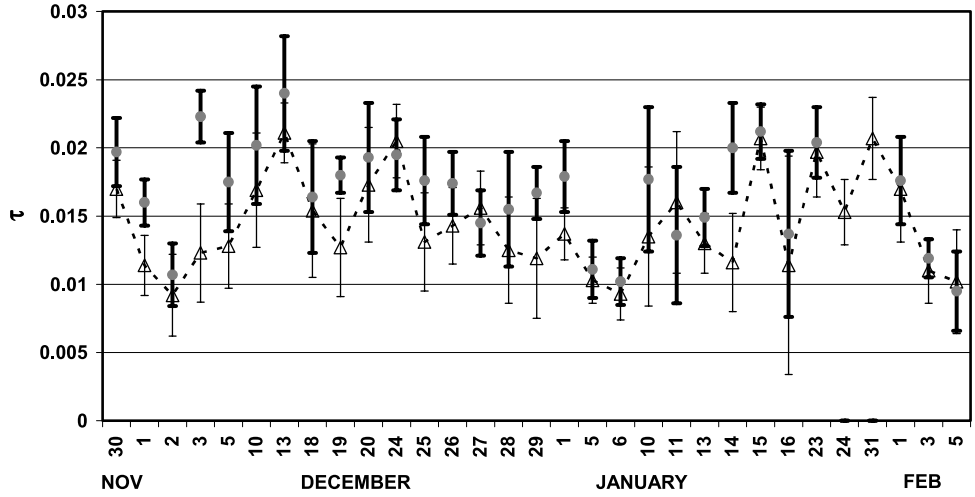

Figure 2. Time patterns of the daily mean values of aerosol optical thickness τ at wavelength λ = 500 nm, determined during the campaign: The average values determined over the morning and the evening time intervals are represented with open triangles, while the average values of τ determined over the middle part of the day are given by solid squares. Vertical bars give the corresponding standard deviation values.

visible wavelengths. Because of the presence of snowfields in the numerous hollows of the irregular terrain around Campo Icaro, the effects due to the clean snowfields were taken into account. We considered that for this surface, the albedo presents values mostly ranging between 0.75 and 0.90 with a mean value of 0.8, as shown by *Zibordi et al.* [1996] and *Lupi et al.* [2001] from surface reflectance measurements taken in various snow covered and iced areas, not far from TNB. Thus, assuming that only one third of the area surrounding Campo Icaro is covered by snow and the rest is a rocky surface without snow, we estimated a value of A close to 0.4.

4. Results

[20] Using the Skyrad code, an important criterion is to reject the results obtained with retrieval errors ε_R higher than 5% [*Nakajima et al.*, 1983]. In our case, because of the low values of aerosol optical thickness τ measured in Antarctica, values of ε_R were found to be generally higher than 5% and mostly between 5% and 15%. Greater uncertainties were recorded for optical thickness τ lower than 0.01. For this reason, we decided to avoid the rejection of data with $\varepsilon_R > 5\%$, considering also the data with ε_R varying between 5% and 15%, in all cases where the corresponding best fit solutions were found to be stable in time. This implies that the retrieval of aerosol characteristics becomes more uncertain, because the inversion algorithm tries to compensate the large error by setting the aerosol parameters unrealistically. So, most of cases presenting values of ε_R larger than 7% could include clouds or rapid changes in aerosol stratification features.

[21] Aerosol optical thickness τ, volume distribution $v(r)$, Ångström exponent α and single-scattering albedo ω showed strong dependence on the air mass m_o and, hence, on the measurement hour. Such dependence features were observed throughout the campaign. Therefore the calculation of only one average value per day of the four above-mentioned parameters was considered unsuitable for studying the evolution of the Antarctic aerosol during the campaign. We decided to determine two mean values for each day, one for the middle part of the day (indicated by subscript 2) and one for the rest of the day (indicated by subscript 1). Air mass value m_o = 2, equivalent to solar zenith angle $\theta_o = 60°$, was chosen to establish the limits of the middle part of the day, during the period from 30 November to 20 January, and m_o = 2.2, corresponding to $\theta_o = 63°$, from 24 January to 5 February. With this choice, each of the two daily mean values was computed over a time interval of about 8 hours. Moreover, considering only the measurements taken with $m_o > 4.5$, we avoid analyzing the data obtained in the presence of possible scintillation effects or altered by inaccurate evaluations of air mass m_o.

4.1. Optical Thickness

[22] During the whole campaign, the values of τ, retrieved from the inversion of $R(\lambda, \Theta)$ data, were found to be very low, ranging between about 0.01 and to 0.02 at wavelength λ = 500 nm (Figure 2). These values of aerosol optical thickness agree very well with previous results determined by *Shaw* [1982] and *Matsubara and Kawaguchi* [1983], who found background values of Antarctic optical depth ranging between 0.01 and 0.03.

[23] The diurnal behavior of this quantity was characterized by higher values during the middle of the day, and by gradually decreasing values in the early morning and late afternoon, as parameter m_o increases (Figure 3). The coefficient of correlation CORR between m_o and τ was also calculated during the campaign, as can be seen in Figure 4, confirming this tendency, since values of CORR greater than 0.6 were generally found.

4.2. Ångström Coefficient

[24] We also computed two daily average values of the Ångström coefficient α [*Ångström*, 1964], using all the measurements of τ carried out at the four wavelengths. In

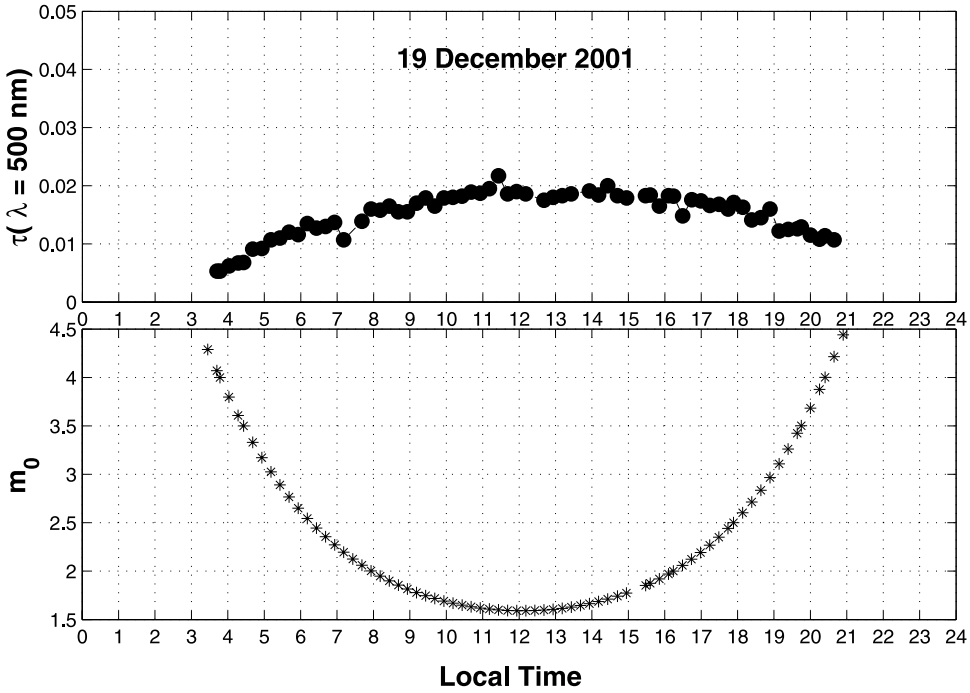

Figure 3. (top) Diurnal time patterns of the aerosol optical thickness τ measured at the 500 nm wavelength, on 19 December 2001. (bottom) Diurnal time patterns of the air mass m_o on the same day. Local time is given by the UTC time plus 11 hours.

Table 1, mean values of parameter α are given for all the measurement days of the campaign. The large variability of the values from one day to another is mostly due to the different humidity conditions, which usually exert a strong influence on particle size. The diurnal time patterns of this parameter were found to present values of α_1 greater than α_2, indicating that an increase in the large particle content took place during the middle part of the day.

4.3. Volume Distribution

[25] The volume size distributions, defined as the volume occupied by aerosol in the air column of unit cross section within the unit logarithmic radius interval (measured in cm^3/cm^2), were generally found to present bimodal shapes, characterized by two well-defined peaks with maximum values within the radius intervals $0.1 \leq r_1 \leq 0.3$ μm and $5 \leq r_2 \leq 7$ μm, respectively, as shown in the examples in Figure 5. *Shettle and Fenn* [1979] and *d'Almeida et al.* [1991] pointed out that the two modes are respectively typical of the accumulation mode, consisting mainly of soot and sulfate particles, and the coarse mode, formed by sea-salt particles growing because of relative humidity conditions higher than 60%, as frequently encountered during the campaign. The values

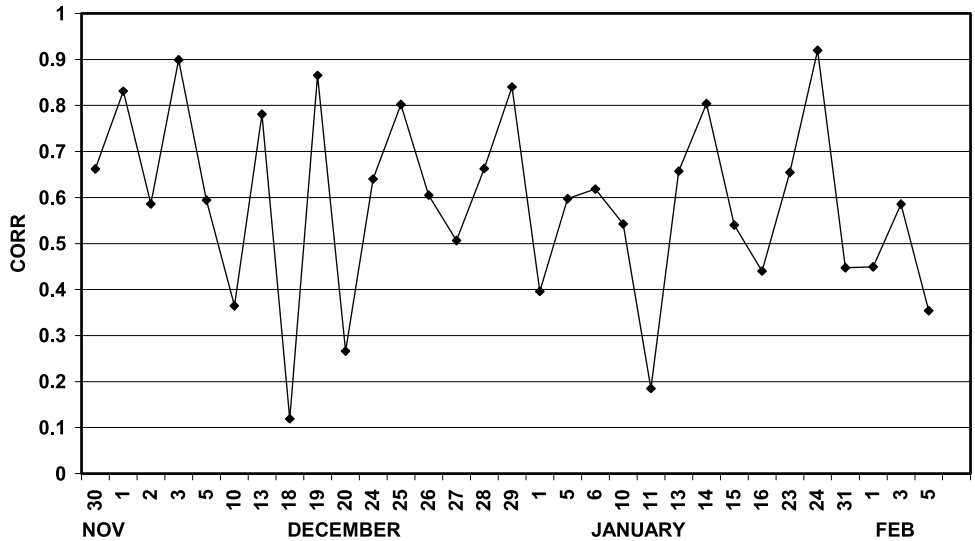

Figure 4. Time patterns of the daily mean values of correlation coefficient CORR between optical air mass m_o and aerosol optical thickness τ measured at the 870 nm wavelength during the campaign.

Table 1. Mean Daily Values of the Ångström Coefficient α Determined During the Campaign[a]

Day	α_1	α_2
30 Nov.	0.80	0.64
1 Dec.	0.55	0.50
2 Dec.	0.50	0.41
3 Dec.	0.69	0.86
5 Dec.	0.78	0.63
10 Dec.	0.77	0.58
13 Dec.	1.17	0.95
18 Dec.	0.67	0.66
19 Dec.	0.57	0.53
20 Dec.	0.70	0.57
24 Dec.	0.85	0.27
25 Dec.	0.69	0.65
26 Dec.	0.85	0.69
27 Dec.	0.99	0.64
28 Dec.	0.74	0.57
29 Dec.	0.71	0.56
1 Jan.	0.45	0.55
5 Jan.	0.49	0.26
6 Jan.	0.39	0.19
10 Jan.	0.52	0.32
11 Jan.	0.50	0.24
13 Jan.	0.41	0.20
14 Jan.	0.34	0.23
15 Jan.	0.44	0.38
16 Jan.	0.47	0.31
23 Jan.	0.87	0.51
24 Jan.	0.63	999
31 Jan.	1.11	999
1 Feb.	0.77	0.80
3 Feb.	0.88	0.51
5 Feb.	0.42	0.28

[a]Parameter α_1 gives the mean values determined over the morning and evening time intervals, and parameter α_2 gives the mean values determined over the middle part of each day.

of the two mode radii were found to be rather stable in time, whereas the coarse volume concentration $v(r_2)$ varied considerably with time, throughout the day. This is clearly shown in Figure 5, where three volume size distributions are presented for three different times of the same day, i.e., morning, noon and afternoon. It can be seen that a more pronounced maximum of the coarse volume concentration is present at noon, whereas the accumulation particle volume concentration $v(r_1)$ exhibits more limited variability features during the day. The stability of the concentration and mass mean radius of the accumulation mode over a three-week period in the Antarctic austral summer of 1995 was also reported by *Hillamo et al.* [1998], who found that the coarse mode was subject to vary significantly during that period, in good accordance with the present results.

[26] On the various measurement days of the campaign, the coarse mode made the most important contribution to the columnar aerosol volume load. In fact, ratio $v(r_1)/v(r_2)$, calculated dividing the volume concentration determined at mode radius r_2 by the volume concentration at mode radius r_1, generally followed a diurnal trend, with values fluctuating between 0.05 and 0.08 until the early afternoon, and then increasing up to about 0.15, as a result of the gradual decrease of $v(r_2)$ during the last hours of the day.

4.4. Refractive Index and Single-Scattering Albedo

[27] The two daily mean values for the real part m of the refractive index retrieved for the entire campaign are shown in Figure 6. Parameter m generally showed a slight diurnal variability, with standard deviation values lower than 6.5% for most days. The variability was higher over the whole

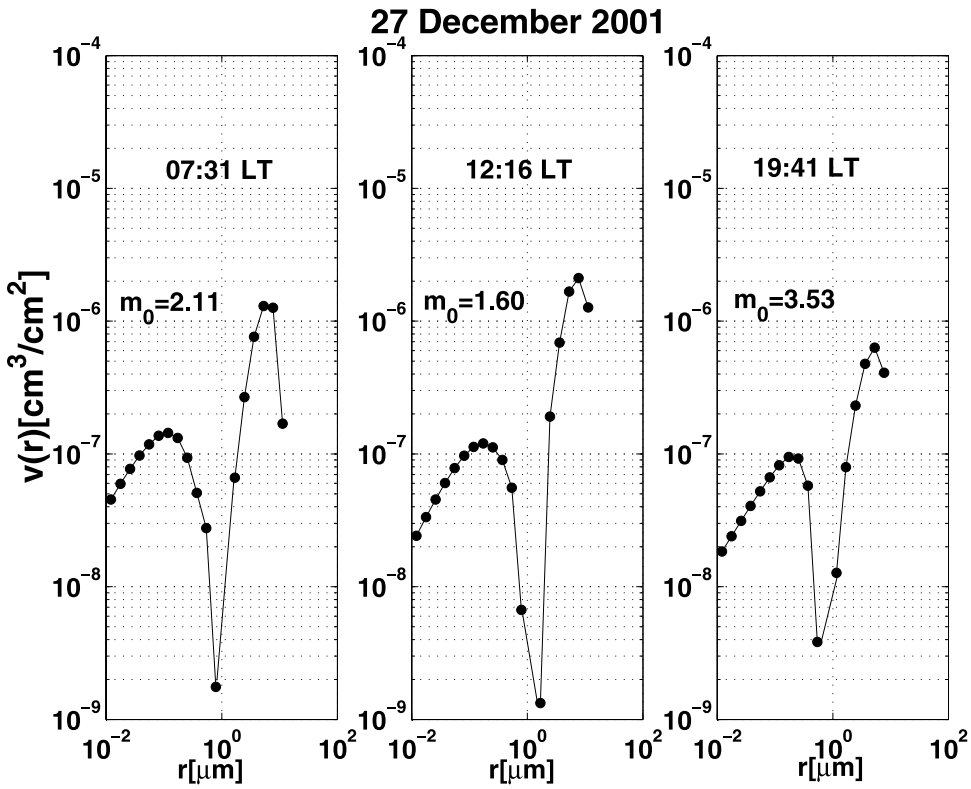

Figure 5. Aerosol volume distribution curves retrieved at three different hours on 27 December 2001.

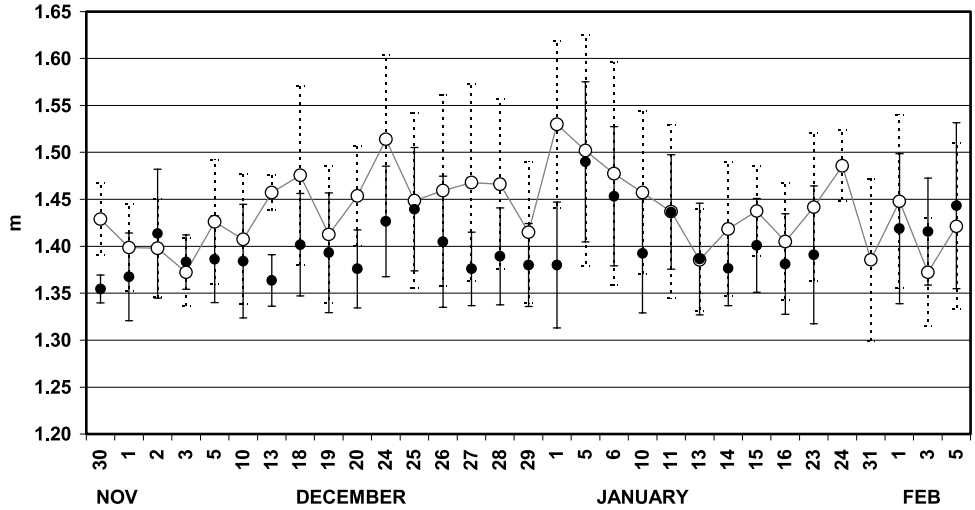

Figure 6. Time patterns of the daily mean values of real part m of particulate refractive index during the campaign: The average values determined over the morning and the evening time intervals are represented with open circles; the average values relative to the middle part of the day are represented with solid circles. Vertical bars give the corresponding standard deviation values.

campaign, especially for m_1, in spite of the stability of aerosol composition expected in Antarctica.

[28] In order to obtain a value of m which can be properly used to characterize the mean chemical composition features of local aerosols, we calculated an average value over the whole campaign, using only the data of m_2, which should be more stable with time, as pointed out above, rejecting the values determined with standard deviations greater than 6.5%. An average estimate giving $\tilde{m} = m - i\,k$ was determined from the data selected following the above criteria, with real part m equal to the average value given in Table 2, which agrees very well with the value $m = 1.41$ proposed in the radiative aerosol model of *Shettle and Fenn* [1979] for oceanic aerosols growing at RH = 70%.

[29] More uncertain results were achieved for the imaginary part k of the particulate refractive index. The values of k obtained from the above calculations turn out to show a strong diurnal variability both daily and over the whole campaign, as can be seen in Figure 7. Through the present analysis, an overall average value of k equal to 0.02 ± 0.01 was retrieved, together with an overall average value of ω, equal to 0.751 ± 0.065 at the 500 nm wavelength, as shown in Table 2.

5. Discussion of the Results

[30] As shown in section 4, aerosol optical thickness was found to have a typical diurnal behavior increasing during the early morning and subsequently decreasing throughout the late afternoon. These time variations can be reasonably attributed to the transport of particulate matter associated with the intense convective motions generated by the solar heating of the dark and de-iced soil during the middle part of the day. Such convective motions cause the increase of the boundary layer depth, as shown by acoustic soundings performed in previous campaigns [*Mastrantonio et al.*, 1989; *Viola et al.*, 1996], and generate a more intense vertical transport of aerosol particles from the ground into the atmosphere. Such features can be explained, at least in part, in terms of gas-to-particle conversion processes caused by the ground surface drying due to solar heating.

[31] The correlation coefficient values calculated between air mass m_o and optical thickness τ were found to be in general greater than 0.6, and lower than 0.6 in particular cases when sharp hourly variations in relative humidity conditions were observed during the day. Considering that hygroscopic particles grow appreciably with increasing RH [*Hänel*, 1976], the aerosol optical thickness is expected to depend not only on the mass loading of airborne particles within the vertical atmospheric column, but also to vary considerably as a function of RH, because of both usually large variations in the liquid water mass fraction and correspondingly marked changes in the overall refractive index of aerosol particles. Thus abrupt changes in aerosol optical thickness are expected to occur for sudden variations in RH, masking its correlation with the time of the day.

[32] The diurnal time patterns of the Ångström coefficient highlighted the increasing content of large particles during the middle part of the day. Since marked variations in RH were generally not observed in these hours, the above increase can be reasonably explained by the arrival of more weighty contents of large particles due to a more intense transport of fresh aerosol particles, and not in terms of growth of existing particles by condensation.

[33] In agreement with these results, the coarse volume concentration showed a gradual decrease during the late afternoon when a lower temperature was usually observed

Table 2. Mean Values of the Real Part m and the Imaginary Part k of Particulate Refractive Index Retrieved From All the Measurements Taken During the Campaign, Together With the Mean Value of Single-Scattering Albedo ω Obtained at the 500 nm Wavelength

	Mean Value Retrieved During the Campaign
m	1.40 ± 0.02
k	0.02 ± 0.01
$\omega(\lambda = 500$ nm)	0.751 ± 0.065

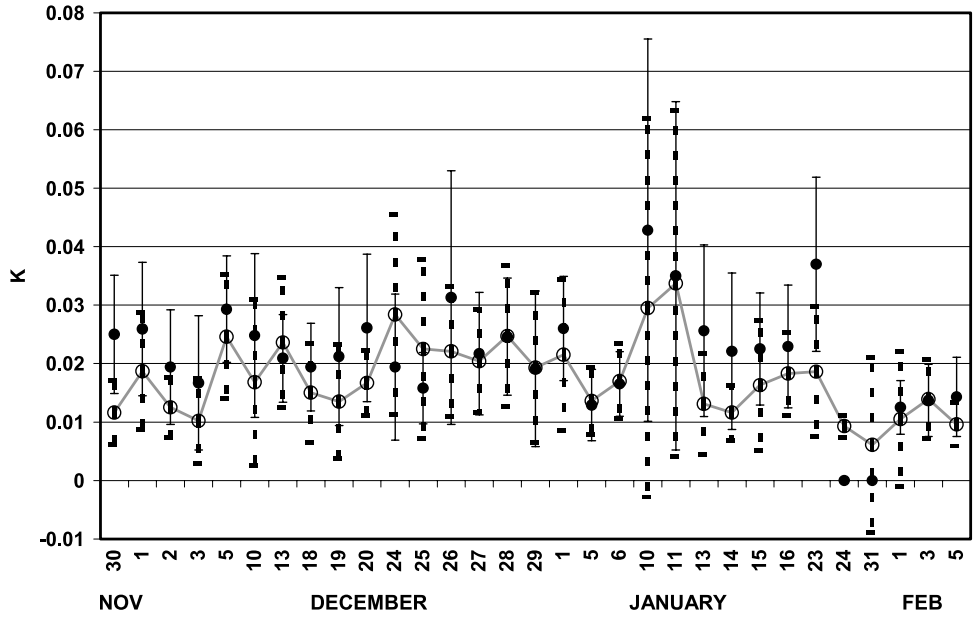

Figure 7. Time patterns of the daily mean values of the imaginary part *k* of particulate refractive index during the campaign: The average values determined over the morning and the evening time intervals are represented with open circles; the average values over the middle part of the day are represented with solid circles. Vertical bars give the corresponding standard deviation values.

at ground level together with less intense convective motions. This weakening of the convective regime during the afternoon is expected to be associated with a gradual decrease in the transport of aerosol particles from the ground into the atmosphere.

[34] As described in section 4, we retrieved the Antarctic aerosol characterized by a bimodal volume size distribution with an accumulation mode radius of 0.1–0.3 μm, and a coarse mode radius of 5–7 μm. These results are confirmed by the measurements performed by *Hillamo et al.* [1998] through the analysis of particulate samplings taken at the Terra Nova Bay station. They showed that the aerosol size distribution curves exhibit multimodal features, with two submicron and two supermicron modes. The first submicron mode was found to contain particles that can be generated in part by gas-to-particle conversion processes, closely related to the surface drying caused by the solar heating of the ground [*Gras*, 1983]. It was found to have an average mean radius of about 0.035 μm, producing such weak optical effects as to be undetected with our method. Conversely, the second submicron mode presents an average mean radius of about 0.15 μm and closely corresponds to the accumulation mode retrieved by our technique. It was found to contain a predominant fraction of sulfates and a more limited fraction of sea-salt particles. Of the two coarse particles modes found by *Hillamo et al.* [1998] in the supermicron size range, the first was estimated to have an average mode radius of around 1 μm and the second an average radius of about 3.5 μm. Both modes contain a predominant fraction of sea-salt ions, and small percentages of sulfates and nitrates. Comparing these results with our findings, the above modal radii turn out to be overestimated by our technique. The discrepancies could be due to the fact that the first results refer to ground-level particle samplings, whereas our findings were obtained from measurements carried out along the vertical atmospheric path.

[35] Although not all the size distribution features determined by us and *Hillamo et al.* [1998] are found to be in close agreement, the observed predominance of the coarse mode over the accumulation mode, as defined by our results, matches very well the overall average composition features of the multimodal size distribution curve of particulate matter given by *Hillamo et al.* [1998], who found a composition of 75% sea-salt particles, and 25% sulfates and nitrates. The chemical analysis measurements carried out by *Teinilä et al.* [2000] and *Kerminen et al.* [2000] at the Finnish station Aboa in western Queen Maud Land, Antarctica, during the austral summer showed very similar results.

[36] Methane sulphonate (MSA) is also present in the Terra Nova Bay atmosphere, because of dimethylsulphide (DMS) oxidation, DMS being released from the sea. In addition, minor concentrations of other particulate compounds are expected to be present, because of (1) some ammonia produced by the penguin population present in this coastal area, through the decomposition of excreted organic nitrogen compounds [*Gras*, 1983]; (2) volcanic particles due to the plume of Mount Erebus, as shown by *Shaw* [1980] and confirmed by local measurements of the radon (^{222}Rn) concentration carried out at Terra Nova Bay over the last years [*Tositti et al.*, 2002]; and (3) soot (black carbon) as found by *Wolff and Cachier* [1998] in Antarctic coastal areas at the same latitudes, with relatively low concentrations in December and January, showing patterns controlled by the timing of biomass burning in the tropics, strongly modulated by the efficiency of transport to Antarctica. The assumption of these minor particulate matter types could allow us to explain in part the rather high values

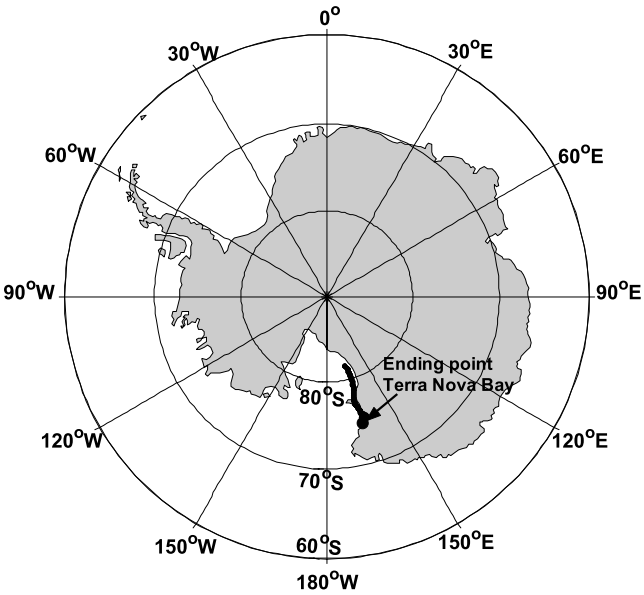

Figure 8. Ninety-six-hour backward trajectories ending at TNB on 29 December 2001, at 1300 LT. The two trajectories calculated at the 500 m and 1000 m levels are in practice coincident.

of the imaginary part k and the very low values of single-scattering albedo found above.

[37] The analysis of the backward trajectories, produced over sea with the HYSPLIT model provided by the NOAA Air Resources Laboratory indicates the large presence of marine aerosols. The backward trajectory analysis showed that most of the trajectories passed over the Ross Sea. Figure 8 shows an example of a backward trajectory of 96-hour duration ending at Campo Icaro.

[38] The sensitivity of the retrieved trajectories to the orography approximation used in the HYSPLIT model was also checked. The meteorological data required to calculate background trajectories correspond to average grid cell values. In our case, there are large terrain gradients near the experimental site and, hence, the average terrain for the grid cell containing the station is very unrepresentative. Without meteorological data of higher spatial resolution, a perfect solution cannot be obtained. The meteorological data are archived in pressure coordinates, and although the initial computed low-level trajectory will be correct near the ground (because the effects of surface friction are included), as soon as the trajectory moves away from the surface, the wind will correspond with the appropriate model terrain pressure level. Thus, in order to check the sensitivity of the results with respect to the orography approximation, we computed two backward trajectories for the same time, one ending at the correct station location and the other ending at a location just far enough away as to have a sea level terrain height. Both trajectories were found to be nearly coincident, indicating a good level of confidence in these results.

[39] As mentioned in section 4, we encountered considerable difficulties in applying the retrieval procedure of the refractive index using the Skyrad code; this problem is probably related to the particularly clean air conditions of the Antarctic atmosphere observed on our measurement days. In fact, the retrieval of the refractive index is based on the inversion of the data of normalized radiance R, expressed in terms of equation (3). Since R is given with good approximation by the product $\omega\ \tau\ P$, in all cases of very clean air conditions of the atmosphere, where optical thickness τ assumes values of the order of magnitude of 0.01, the physical quantity to be inverted is generally very small. Subject to increase by multiple scattering, the signal given by the imaginary part of the refractive index is not large on our days with respect to the turbid atmosphere cases, rendering its retrieval rather difficult. On this matter, it could also be important to point out that a slight error in the calibration constant F_o of the radiometer can cause a large error in the imaginary part k in such a clean atmosphere, leading to overestimation errors.

[40] Considering the percentage composition of aerosol described above and increasing the mass percentages of minor substances from 0 to 1%, we assumed the values of refractive index proposed for the various particulate components by *Hänel* [1976], *Vermote et al.* [1997], *Volz* [1973], and *Patterson* [1981] and found that m varies thorough the range 1.42–1.55, which actually includes most of the values retrieved by us. Concerning the imaginary part k, we found that it can vary within the range from 0.0014 to 0.026, which turns out to include most of the values retrieved using the present method.

[41] Concerning the single-scattering albedo ω, it was found to be appreciably lower than expected for Antarctic aerosols. In fact, according to *Takemura et al.* [2002], we determined values of ω ranging mostly between 0.92 and 0.94, through calculations made for predominant contents of nonabsorbing sea-salt and sulfate aerosols, combined with a relative concentration of 0.2% black carbon, transported from the tropical and midlatitude regions, as shown by *Wolff and Cachier* [1998]. Unfortunately, no in situ measurements were available to substantiate the significant presence of this particulate type.

6. A Case Study of Katabatic Wind

[42] In Antarctica, the subsidence of air masses over the Plateau and loss of radiative energy during most of the year are the main causes of the formation of strong temperature inversions near the surface in the interior of the continent. This situation induces the cold air masses to move away from the subsidence areas toward the coastal areas, following orographic reliefs and converging into a few limited areas, called confluence zones, where the wind speed usually reaches high values. This kind of strong flow of air masses from the interior to the coastal regions is referred to as katabatic wind. In the TNB area, the katabatic flows come from the Reeves and Priestley Glaciers.

[43] During the campaign, the wind measurements recorded by the AWS station showed three clear events of katabatic wind, on 10, 11 and 16 January 2002. The three cases were closely in order to investigate the influence of katabatic wind on Antarctic aerosol. Figure 9 shows a backward trajectory for the event of 11 January 2002, indicating very clearly that the air masses originated from the interior of the continent, on that day.

[44] The day of 16 January was characterized by high-relative-humidity conditions at the ground in the early

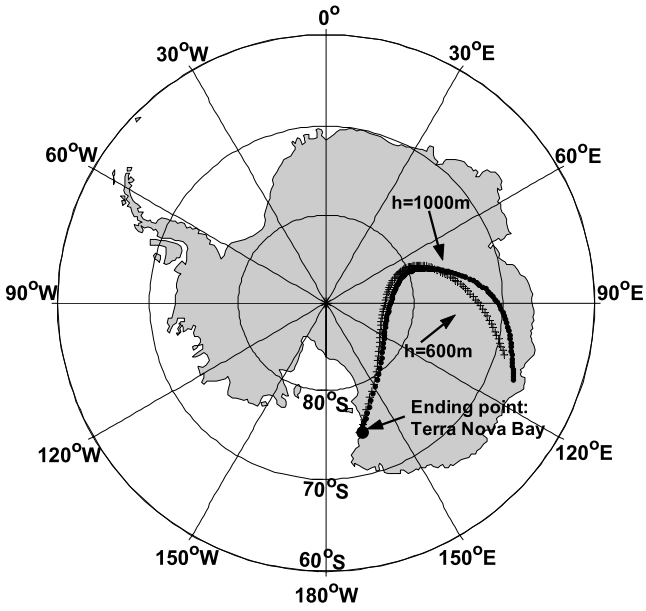

Figure 9. Ninety-six-hour backward trajectories ending at TNB on 11 January 2002 at 1300 LT.

morning (RH exceeding 70%) and by the absence of wind. The wind started to blow in the late morning, with increasing speed until reaching 15 m s^{-1} at the end of the day. In this case, because of the short duration of the katabatic event, it was not possible to verify accurately if the local aerosol composition was subject to important changes. What we noticed was that a rapid decrease took place in the relative humidity from 80% to 30%, plausibly as a result of the increase in wind speed, causing the mixing of the air masses and bringing about the redistribution of water vapor toward the higher layers. Events of this kind can strongly affect particle size [*Hänel*, 1976]. Thus higher values of the aerosol optical thickness τ, equal to 0.02 at visible wavelengths, were observed in the early morning, gradually decreasing throughout the middle part of the day to reach the lowest value of 0.0075 (Table 3). The coarse particle mode radius decreased from r_2 = 7.34 μm during the early hours of the day to r_2 = 5.30 μm after noon. Correspondingly, the accumulation particle mode radius r_1 remained substantially unvaried during that day. Thus relatively smaller values of the imaginary part k were retrieved during the morning compared to the early afternoon, when RH assumed particularly high values together with slightly higher values of the single-scattering albedo.

[45] The katabatic wind episode of 10 and 11 January was found to be of greater interest. The katabatic wind started to blow from NE at 1800 LT on 9 January, reaching its maximum speed of 28 m/s at 0600 LT on 10 January, the local time (LT) being given by UTC + 11 hours. It then remained quite stable in both intensity and direction until 0500 LT on 12 January. Figure 10 provides evidence of the marked lowering in atmospheric aerosol loading caused by the wind. The aerosol optical thickness τ exhibits the typical diurnal behavior, presenting higher values during the middle part of the day, while its daily maximum values were found to decrease from 10 January until the morning of 12 January. In fact, a wind blowing from the Antarctic interior (completely covered by ice) toward the coastal site should not contribute very much to increasing the crustal/continental aerosol component, while it should certainly lower the marine aerosol component. Together with the effects due to the decreasing RH, the change in the transport features associated with katabatic wind could be a plausible explanation of the observed decrease in optical thickness.

Table 3. Average Values of Relative Humidity RH, Aerosol Optical Thickness τ at the 500 nm Wavelength, Single-Scattering Albedo ω at the Same Wavelength, Real Part m and Imaginary Part k of Columnar Particulate Refractive Index, and Coarse Particle Mode Radius r_2 Relative to the Days Without Katabatic Wind (Wind Speed < 2 m/s) and Days With Katabatic Wind (Wind Speed > 10 m/s)

	Retrieved Value Without Katabatic Wind	Retrieved Value With Katabatic Wind
Wind intensity, m/s	<2	>10
RH, %	80	30
τ	0.02	0.0075
ω	0.75	0.65
m	1.40	1.45–1.50
k	−0.015	−0.025
r_2, μm	7.34	5.3

[46] To highlight the main differences between the local aerosol features with and without katabatic wind, the results obtained on two days characterized by katabatic wind were compared with those observed on four consecutive ordinary days (from 26 to 29 December 2001), selected to represent the standard weather conditions encountered during the campaign and, hence, to describe the local aerosol characteristics in the absence of katabatic wind.

[47] The ratio $\nu(r_1)/\nu(r_2)$ between the aerosol loadings of the fine and coarse particle fractions was found to assume smaller values during the days with katabatic wind. This was mostly due to the marked decrease of $\nu(r_1)$ both in the middle part of the day (V_1) and in the morning and afternoon (V_2), as clearly shown on 11 January in Figure 11a, combined with the stable time patterns of $\nu(r_2)$, as can be seen in Figure 11b. On 12 January, only morning data were available, but the sudden decrease of about 50% observed for all the three curves in Figure 11a on 11 January strongly suggests the above explanation in terms of katabatic wind effect is reasonable. The error bars are not given

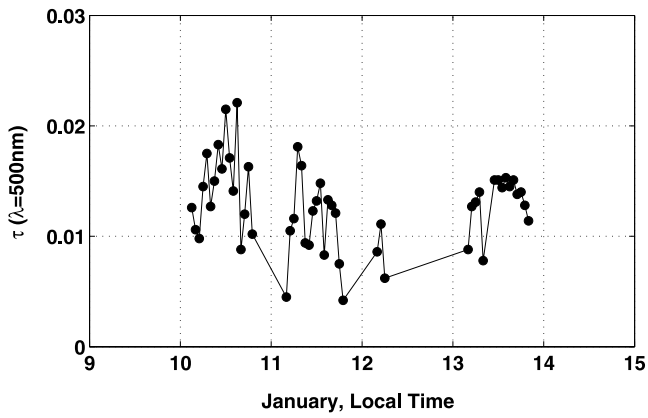

Figure 10. Average time patterns of aerosol optical thickness τ at the 500 nm wavelength, obtained from the data taken on the katabatic wind days of January 2002.

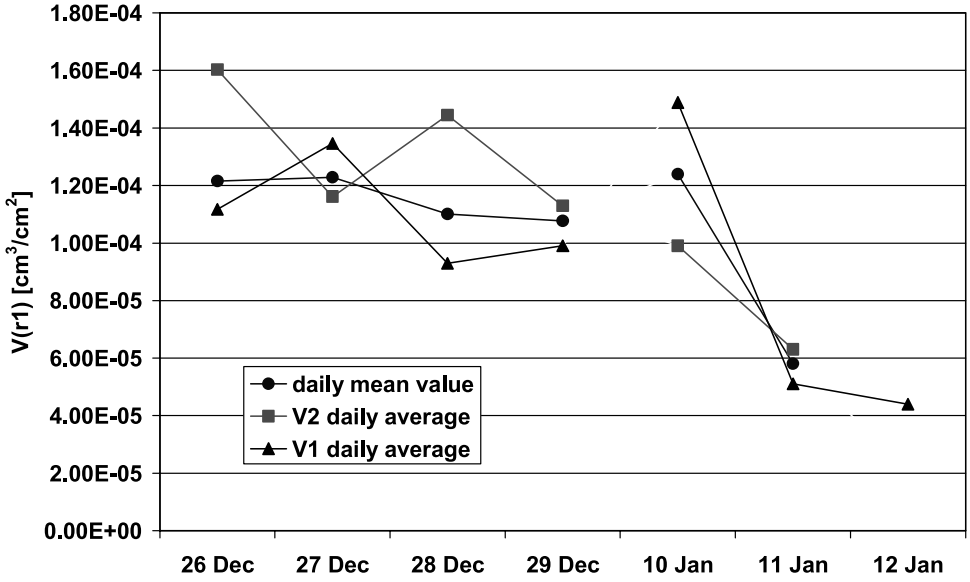

Figure 11a. Daily mean values of volume concentration of the fine particle mode obtained on 4 ordinary days of December, compared with those determined on the 3 days of January with katabatic wind. Solid circles refer to the daily mean values, solid squares refer to the average values determined over the morning and evening time intervals, and solid triangles refer to the average values determined over the middle part of the day.

in Figures 11a and 11b, since they are of comparable magnitude with the estimates of both parameters $v(r_1)$ and $v(r_2)$. However, in spite of the large errors, the stable results obtained at different hours of each day allow us to attribute confidently a physical meaning to the measurements. In fact, the fine mode is the product of oxidization of sulfuric gaseous compounds emitted by the ocean and even by air pollution sources far from Antarctica. Thus, considering that the katabatic wind pushes maritime air mass away from the observation site, the gradual decrease of $v(r_1)$ may be correctly explained in terms of marine particle removal. With regard to the stability of the time patterns of $v(r_2)$, it is worth pointing out that a serious question must be considered, since the coarse particle mode could sometimes be an artefact of the instrumentation. Under such a small aerosol loading, an undesirable reflection of direct solar radiation at the internal surface of the light-shading hood of the instrument could cause a fictitious coarse mode. The first mode radius was found to be slightly larger, within the 0.2–0.4 μm range, on the katabatic wind days, whereas r_2 assumed

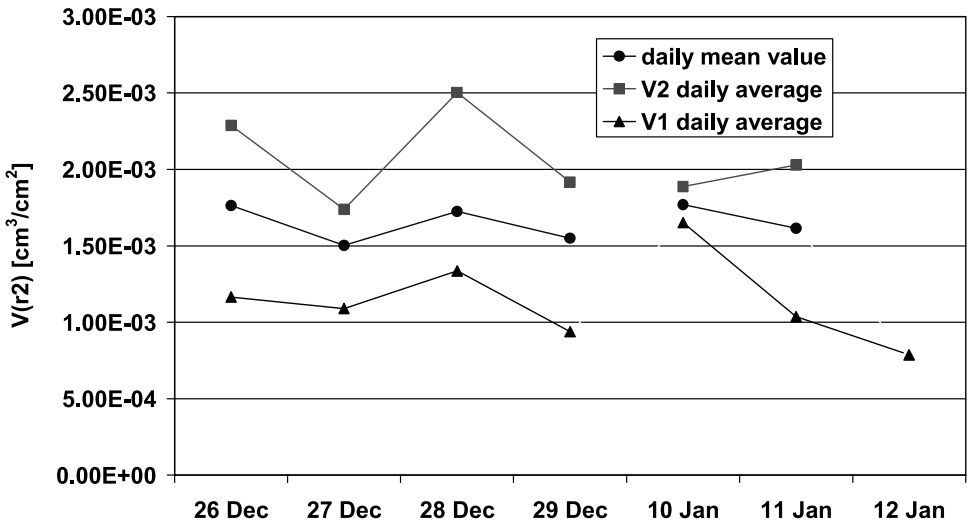

Figure 11b. Daily mean values of volume concentration of the coarse particle mode on 4 ordinary days of December, compared with those determined on the 3 days of January with katabatic wind. Solid circles refer to the daily mean values, solid squares refer to the average values determined over the morning and evening time intervals, and solid triangles refer to the average values determined over the middle part of the day.

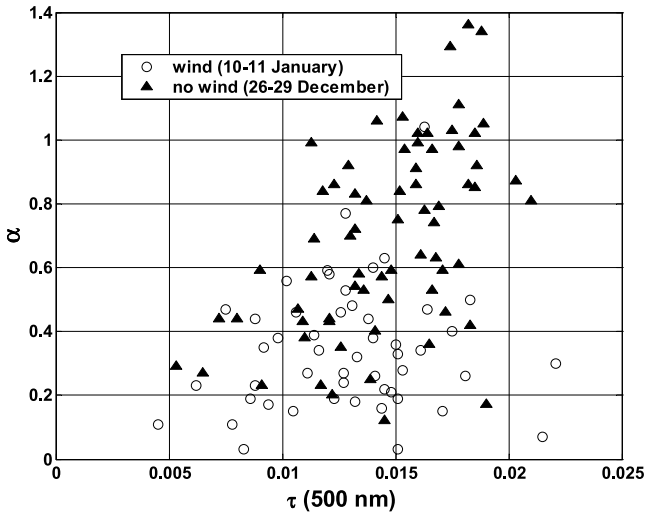

Figure 12. Scatter diagram of the Ångström coefficient α versus the aerosol optical thickness τ measured at the 500 nm wavelength. Open circles refer to days with katabatic wind (10 and 11 January 2002), and solid triangles refer to days without katabatic wind (26–29 December 2001).

rather stable values. Moreover, the wind caused a decrease in RH, sometimes reaching values lower than 30%. This change in the RH also caused a decrease in the liquid water content of the particles. Consequently, the retrieval of the real part of the particulate refractive index led us to obtain values of m ranging between 1.45 and 1.50 on 11 January 2002, which are appreciably greater than the value of m = 1.40 previously proposed in Table 2 as a mean characteristic of the Antarctic aerosol.

[48] The katabatic wind resulted from our analysis to be a mechanism causing both marine aerosol removal from the local atmosphere above the Campo Icaro coastal site, and the transport of smaller amounts of larger and drier particles from the interior of the continent. In fact, we observed that (1) the aerosol optical thickness decreased; (2) the real part of refractive index increased, clearly demonstrating that the water mass fraction underwent a decrease; (3) the fine particle mode features changed, indicating the arrival of larger particles, since $v(r_1)$ was found to decrease while radius r_1 increased and the corresponding number concentration decreased; and (4) the coarse particle mode did not apparently change either in volume or mode radius.

[49] In addition, it is realistic to assume that the transported particles could be of different composition before and during the katabatic episode: of marine origin and with higher liquid water content in the former period, and with stable sizes and consisting of drier substances of different origin in the latter, as indicated by the increase of real part m of the refractive index. In fact, the percentage content of crustal particulate (silicates, porphyries, syenogranites and basalts) from the rocky outcrops above the ice cap increases on days with katabatic wind, while the sea-salt content decreases.

[50] The above explanation of aerosol parameter changes due to katabatic wind effects on the particulate matter composition agrees very well with the evaluations of the Ångström coefficient shown in Figure 12: Parameter α assumed lower values during the days with katabatic wind, which are usually characterized by lower values of optical thickness τ, compared to those measured on days without wind. This behavior suggests the presence of larger particles in katabatic wind conditions.

7. Conclusions

[51] The columnar optical characteristics of Antarctic aerosol were retrieved from the set of direct and diffuse solar irradiance measurements performed at Terra Nova Bay during the austral summer 2001–2002. During the campaign, temperature values varying between −4°C and 10°C were recorded at the ground, which turned out to be appreciably higher than those measured in previous years. Relative humidity of air varied between 30% and 80%, without presenting a regular behavior related to a typical diurnal cycle.

[52] The Skyrad code was used to apply the inversion procedure to the irradiance measurements, providing the following results.

[53] 1. Aerosol optical thickness at 500 nm wavelength was evaluated to vary mainly between 0.01 and 0.02 on the measurement days; the diurnal trend was characterized by a regular increase throughout the morning, attaining the highest values in the middle of the day, probably because of intense convective motions, followed by a gradual decrease during the afternoon.

[54] 2. The Ångström coefficient varied considerably from one day to another, presumably because of the large variations in RH in the low atmosphere. The daily time patterns of the optical parameters highlighted the presence of a high amount of large particles along the Sun path during the middle part of the day, due to the vertical transport of fresh aerosols by convective motions.

[55] 3. The volume size distribution curves showed clear bimodal features. The accumulation mode radius varied mainly within the 0.1–0.3 μm radius interval, indicating the presence of soot and sulfate particles, in agreement with local in situ measurements of particulate matter composition. The coarse mode radius assumed values ranging between 5 and 7 μm, providing evidence of the presence of sea-salt particles. During the campaign, the coarse mode was estimated to make the most important contribution to the vertical aerosol loading, confirming that the local aerosol consists mainly of marine particles in the absence of katabatic wind effects.

[56] 4. The real part of the refractive index revealed a slight diurnal variability, with an overall average value equal to 1.40 ± 0.02 characterizing the Antarctic aerosol polydispersions.

[57] 5. The inversion procedure used to analyze field measurements with the aim of determining the imaginary part of refractive index yielded not unrealistic results, in spite of the problems due the application of the technique in a very clean atmosphere. The mean value k = 0.02 ± 0.01 was obtained, which is consistent with the values obtained by us on the basis of the chemical composition features of Antarctic aerosol particles found by *Hillamo et al.* [1998] and *Wolff and Cachier* [1998].

[58] 6. The mean value of single-scattering albedo at the 500 nm wavelength was 0.751 ± 0.065, which turns out to

be considerably lower than expected for Antarctic aerosols and the values calculated above for the composition features assumed according to the *Hillamo et al.* [1998] findings, though we do not have in situ measurements suitable for demonstrating that particulate matter strongly absorbing the solar radiation is present along the Sun path.

[59] The last two results are affected by serious difficulties in correctly applying the Skyrad code in the very clean air conditions of the Antarctic atmosphere, where the signal to be inverted is actually very small. This tends to be confirmed also by the rather high values of the retrieval errors (up to 15%) obtained in the present measurements, when compared with results found for more turbid air conditions, where errors do not usually exceed 5–7%.

[60] A katabatic wind episode was also analyzed to study the changes in the radiative properties of local aerosol caused by the strong winds blowing from the interior. The advection of larger and drier fresh particles from the inner part of the continent and the removal of suspended marine particles due to the wind cause the decrease in the aerosol optical thickness, as observed during such an event. In fact, the real part of refractive index was observed to increase up to 1.45–1.50 because of katabatic wind, showing a simultaneous decrease in the liquid water content of the aerosol particles and a slight increase of the accumulation mode radius.

Notation

α	Ångström coefficient.
β	Total differential scattering contribution for the single scattering.
CORR	Coefficient of correlation.
δ	Total optical depth.
$\Delta\Omega$	Instrumental solid view angle.
E	Sky diffuse irradiance.
ε_R	Inversion retrieval error.
F	Direct solar irradiance.
F_0	Extraterrestrial solar irradiance.
φ	Azimuth angle.
k	Imaginary part of the refractive index.
λ	wavelength.
$\tilde{m}$	Complex refractive index.
m_0	Optical air mass.
m	Real part of the refractive index.
P	Phase function.
q	Multiple-scattering contribution.
Θ	Scattering angle.
θ_0	Solar zenith angle.
r	Particle radius.
τ	Aerosol optical thickness.
$v(r)$	Volume size distribution.
ω	Single-scattering albedo.

[61] **Acknowledgment.** This research was supported by the Programma Nazionale di Ricerche in Antartide (PNRA) and developed as part of subproject 2003/6.7, "Characterization of Aerosol Induced Climatic Effects in Polar Regions: An Assimilation and Analysis of Multispectral Sun Photometer Data From the POLAR-AOD Network."

References

Ångström, A. (1964), The parameters of atmospheric turbidity, *Tellus*, *16*, 64–75.

Boi, P., G. Tonna, G. Dalu, T. Nakajima, B. Olivieri, A. Pompei, and M. Campanelli (1999), Procedures of calibration and data elaboration in sky radiance measurements, *Appl. Opt.*, *38*, 896–907.

Campanelli, M., T. Nakajima, and B. Olivieri (2004), Determination of the solar calibration constant for a Sun sky radiometer: Proposal of an in situ procedure, *Appl. Opt.*, *43*, 651–659.

d'Almeida, G. A., P. Koepke, and E. P. Shettle (1991), *Atmospheric Aerosols: Global Climatology and Radiative Characteristics*, A. Deepak, Hampton, Va., 561 pp.

Dubovik, O., and M. D. King (2000), A flexible inversion algorithm for retrieval of aerosol optical properties from Sun and sky radiance measurements, *J. Geophys. Res.*, *105*, 20,673–20,696.

Gras, J. L. (1983), Ammonia and ammonium concentrations in the Antarctic atmosphere, *Atmos. Environ.*, *17*, 815–818.

Hänel, G. (1976), The properties of atmospheric aerosol particles as function of the radiative humidity at thermodynamic equilibrium with the surrounding moist air, *Adv. Geophys.*, *19*, 73–188.

Hillamo, R., I. Allegrini, R. Sparapani, and V. M. Kerminen (1998), Mass size distributions and precursors gas concentrations of major inorganic ions in Antarctic aerosol, *Int. J. Environ. Anal. Chem.*, *71*(3–4), 353–372.

Holben, B. N., et al. (1998), AERONET: A federated instrument network and data archive for aerosol characterization, *Remote Sens. Environ.*, *66*, 1–16.

Kerminen, V.-M., K. Teinilä, and R. Hillamo (2000), Chemistry of sea-salt particles in the summer Antarctic atmosphere, *Atmos. Environ.*, *34*, 2817–2825.

King, M. D., D. M. Byrne, B. M. Herman, and J. A. Reagan (1978), Aerosol size distributions obtained by inversion of spectral optical depth measurements, *J. Atmos. Sci.*, *21*, 2153–2167.

Lupi, A., C. Tomasi, A. Orsini, A. Cacciari, V. Vitale, T. Georgiadis, R. Casacchia, R. Salvatori, and S. Salvi (2001), Spectral curves of surface reflectance in some Antarctic regions, *Nuovo Cimento Soc. Ital. Fis. C*, *24*, 313–327.

Mastrantonio, G., R. Ocone, and G. Fiocco (1989), Acoustic remote sensing of the Antarctic boundary layer, in *1st Workshop, Italian Research on Antarctic Atmosphere: Porano, 11 November 1988*, edited by M. Colacino, G. Giovanelli, and L. Stefanutti, *SIF Conf. Proc.*, vol. 20, pp. 137–144, Soc. Ital. di Fis., Bologna, Italy.

Matsubara, K., and S. Kawaguchi (1983), Spectral extinction measured by sunphotometers at Syowa Station, Antarctica, *Mem. Natl. Inst. Polar Res. Spec. Issue Jpn.*, *29*, 85–93.

Michalsky, J. J., J. A. Schlemmer, W. E. Berkheiser, J. L. Berndt, and L. C. Harrison (2001), Multilayer measurements of aerosol optical depth in the Atmospheric Radiation Measurement and Quantitative Links programs, *J. Geophys. Res.*, *106*, 12,099–12,107.

Nakajima, T., and M. Tanaka (1986), Matrix formulations for the transfer of solar radiation in a plane-parallel scattering atmosphere, *J. Quant. Spectrosc. Radiat. Transfer*, *35*, 13–21.

Nakajima, T., and M. Tanaka (1988), Algorithms for radiative intensity calculations in moderately thick atmospheres using a truncation approximation, *J. Quant. Spectrosc. Radiat. Transfer*, *40*, 51–69.

Nakajima, T., M. Tanaka, and T. Yamanuchi (1983), Retrieval of the optical properties of aerosols from aureole and extinction data, *Appl. Opt.*, *22*, 2951–2959.

Nakajima, T., G. Tonna, R. Rao, P. Boi, Y. Kaufman, and B. Holben (1996), Use of sky brightness measurements from ground for remote sensing of particulate polydispersions, *Appl. Opt.*, *35*, 2672–2686.

Patterson, E. M. (1981), Measurements of the imaginary part of the refractive index between 300 and 700 nanometers for Mount St. Helens ash, *Science*, *211*, 836–838.

Shaw, G. E. (1980), Optical, chemical and physical properties of aerosols over the Antarctic ice sheet, *Atmos. Environ.*, *14*, 911–921.

Shaw, G. E. (1982), Atmospheric turbidity in the polar regions, *J. Appl. Meteorol.*, *21*, 1080–1088.

Shettle, E. P., and R. W. Fenn (1979), Models for the aerosols of the lower atmosphere and the effects of humidity variations of their optical properties, *AFGL Tech. Rep., AFGL-TR-79–0214*, 94 pp.

Shiobara, M., M. Tanaka, T. Nakajima, and H. Ogawa (1987), Spectral measurements of direct solar radiation and the sky brightness distribution at Syowa station, Antarctica, in *Atmospheric Radiation: Progress and Prospects: Proceedings of the Beijing International Radiation Symposium, Bejing, China, August 26–30, 1986*, edited by K.-N. Liou and X. Zhou, pp. 629–637, Am. Meteorol. Soc., Boston, Mass.

Takemura, T., T. Nakajima, O. Dubovik, B. N. Holben, and S. Kinne (2002), Single scattering albedo and radiative forcing of various aerosol species with a global three-dimensional model, *J. Clim.*, *15*, 333–352.

Tanaka, M., T. Nakajima, and M. Shiobara (1986), Calibration of a sunphotometer by simultaneous measurements of direct-solar and circumsolar radiations, *Appl. Opt.*, *25*, 1170–1176.

Teinilä, K., V.-M. Kerminen, and R. Hillamo (2000), A study of size-segregated aerosol chemistry in the Antarctic atmosphere, *J. Geophys. Res.*, *105*, 3893–3904.

Tomasi, C., V. Vitale, and G. Zibordi (1990), Antarctic sky diffuse radiance in Sun-photometric measurements, in *2nd Workshop, Italian Research on Antarctic Atmosphere: Porano, 19–20 October 1989*, edited by M. Colacino, G. Giovanelli, and L. Stefanutti, *SIF Conf. Proc.*, vol. 27, pp. 105–119, Soc. Ital. di Fis., Bologna, Italy.

Tonna, G., T. Nakajima, and R. Rao (1995), Aerosol features retrieved from solar aureole data: A simulation study concerning a turbid atmosphere, *Appl. Opt.*, *34*, 4486–4499.

Tositti, L., S. Sandrini, R. Udisti, A. Migliori, E. B. Pereira, M. G. Bettoli, and S. Parmeggiani (2002), Detection of Mt. Erebus plume at Terra Nova Bay, in *9th Workshop, Italian Research on Antarctic Atmosphere: Rome, Italy, 22–24 October 2001*, edited by M. Colacino, *SIF Conf. Proc.*, vol. 80, pp. 277–285, Soc. Ital. di Fis., Bologna, Italy.

Vermote, E., D. Tanrè, J. L. Deuzè, M. Herman, and J. J. Morcrette (1997), Second Simulation of the Satellite Signal in the Solar Spectrum (6S), 6S User Guide Version 2, 218 pp., Lab. d'Opt. Atmos., Univ. des Sci. et Technol. de Lille, Villeneuve d'Ascq, France, July.

Viola, A., et al. (1996), The boundary layer field experiment in the area of Terra Nova Bay, during the summer 1994–1995, in *9th Workshop, Italian Research on Antarctic Atmosphere: Firenze, 6–8 November 1995*, edited by M. Colacino, G. Giovanelli, and L. Stefanutti, *SIF Conf. Proc.*, vol. 51, pp. 11–22, Soc. Ital. di Fis., Bologna, Italy.

Volz, F. E. (1973), Infrared optical constants of ammonium sulphate, Sahara dust, volcanic pumice and flyash, *Appl. Opt.*, *12*, 564–568.

Wolff, E. W., and H. Cachier (1998), Concentrations and seasonal cycle of black carbon in aerosol at a coastal Antarctic station, *J. Geophys. Res.*, *103*, 11,033–11,041.

Zibordi, G., and G. P. Meloni (1991), Correction of bihemispherical reflectance measurements for noncosine response of 2π steradian optics: A methodology and its application to Antarctic surfaces, *Remote Sens. Environ.*, *37*, 55–62.

Zibordi, G., G. P. Meloni, and M. Frezzotti (1996), Snow and ice reflectance spectra of the Nansen Ice Sheet surfaces, *Cold Reg. Sci. Technol.*, *24*, 147–151.

C. Di Carmine and M. Campanelli, Istituto di Scienze dell'Atmosfera e del Clima, Consiglio Nazionale delle Ricerche, Via Fosso del Cavaliere 100, I-00133 Roma, Italy. (m.campanelli@isac.cnr.it)

T. Nakajima, Centre for Climate System Research, University of Tokyo, 4-6-1 Komaba, Meguro-ku, Tokyo 154-8904, Japan.

C. Tomasi and V. Vitale, Istituto di Scienze dell'Atmosfera e del Clima, Consiglio Nazionale delle Ricerche, Via Gobetti 101, I-40129 Bologna, Italy.